Systematic InSAR tropospheric phase delay corrections from global meteorological reanalysis data

R. Jolivet,[1] R. Grandin,[2] C. Lasserre,[1] M.-P. Doin,[2] and G. Peltzer[3,4]

Received 4 July 2011; revised 17 August 2011; accepted 17 August 2011; published 14 September 2011.

[1] Despite remarkable successes achieved by Differential InSAR, estimations of low tectonic strain rates remain challenging in areas where deformation and topography are correlated, mainly because of the topography-related atmospheric phase screen (APS). In areas of high relief, empirical removal of the stratified component of the APS may lead to biased estimations of tectonic deformation rates. Here we describe a method to correct interferograms from the effects of the spatial and temporal variations in tropospheric stratification by computing tropospheric delay maps coincident with SAR acquisitions using the ERA-Interim global meteorological model. The modeled phase delay is integrated along vertical profiles at the ERA-I grid nodes and interpolated at the spatial sampling of the interferograms above the elevation of each image pixel. This approach is validated on unwrapped interferograms. We show that the removal of the atmospheric signal before phase unwrapping reduces the risk of unwrapping errors in areas of rough topography. **Citation:** Jolivet, R., R. Grandin, C. Lasserre, M.-P. Doin, and G. Peltzer (2011), Systematic InSAR tropospheric phase delay corrections from global meteorological reanalysis data, *Geophys. Res. Lett.*, *38*, L17311, doi:10.1029/2011GL048757.

1. Introduction

[2] Synthetic Aperture Radar Interferometry is a well-established and efficient technique to monitor large scale deformations of the Earth's surface. However, the detection of low amplitude deformations remains challenging due to atmospheric signals that spread over a broad range of spatial wavelengths. The dominant contribution to the atmospheric phase delay, which may reach tens of centimeters, comes from the temporal variation of the stratified troposphere [e.g., *Hanssen*, 2001; *Cavalié et al.*, 2007]. As the resulting phase patterns typically mimic the topography, discriminating between atmospheric and deformation signals is particularly difficult in areas where topography and deformation are correlated [*Beauducel et al.*, 2000].

[3] This issue is critical for interseismic strain measurements in active tectonic environments as deformations occur at a slow rate and are often masked by long wavelength topography-related atmospheric signals [e.g., *Elliott et al.*, 2008; *Fournier et al.*, 2011]. This is the case of major active faults in the India-Eurasia collision zone, where sites of expected strain maxima are chiefly collocated with the large topographic steps surrounding the Tibetan plateau (e.g., Altyn Tagh Fault, Kunlun Fault, Main Himalayan Thrust). Stacking or time filtering methods using numerous acquisitions can effectively remove most of the signal induced by the turbulent atmosphere (i.e., random in space and time) [e.g., *Zebker et al.*, 1997; *Schmidt and Bürgmann*, 2003]. However, the long wavelength topography-correlated atmospheric signal has a seasonal component which may be aliased in the temporal sampling of SAR data, resulting in biased estimates of tectonic strain rates [*Doin et al.*, 2009].

[4] Several methods have been proposed to estimate atmospheric phase delay corrections, including local atmospheric data collection [*Delacourt et al.*, 1998], Global Positioning System (GPS) zenithal delay estimations [*Williams et al.*, 1998; *Webley et al.*, 2002; *Li et al.*, 2006a; *Onn and Zebker*, 2006], satellite multispectral imagery analysis [*Li et al.*, 2006b] and assimilation of meteorological data in atmospheric models [*Wadge et al.*, 2002; *Puysségur et al.*, 2007]. Although these methods proved successful and accurate to mitigate part of the atmospheric phase delay, they rely on local data assimilation, which is rarely available.

[5] Alternatively, an empirical phase/elevation relationship can be systematically estimated from the InSAR data, together with orbital residuals and deformation [e.g., *Remy et al.*, 2003; *Biggs et al.*, 2007; *Cavalié et al.*, 2008; *Lin et al.*, 2010]. Still, the inferred phase delay model needs to be simple enough (such as linearly or quadratically related to the elevation) to avoid introducing an unreasonably high number of parameters in the inversion. In addition, this strategy requires that deformation, atmospheric and orbital contributions are uncorrelated to insure a robust estimation of parameters, which is difficult to ascertain. Empirical estimations of the atmospheric phase delay are therefore difficult in situations where deformation and topography are correlated, such as in the India-Eurasia collision zone.

[6] We present here a simple method for systematic stratified delay mitigation based on the global atmospheric model ERA-Interim (hereafter called ERA-I) provided by the European Center for Medium-Range Weather Forecast (ECMWF). *Doin et al.* [2009] validated the use of global atmospheric models for "a priori" estimation of linear phase/elevation relationships, assumed to be homogeneous over a radar scene. We build upon this previous study by estimating the atmospheric phase contribution at each pixel of interferograms by spatially interpolating between ERA-I grid nodes the modeled delay at the pixel's elevation. In the following sections, we explain how to derive phase delay

[1]Institut des Sciences de la Terre, UMR 5275, Université Joseph Fourier, CNRS, Grenoble, France.
[2]Laboratoire de Géologie, UMR 8538, Ecole Normale Supérieure, CNRS, Paris, France.
[3]Department of Earth and Space Sciences, University of California, Los Angeles, California, USA.
[4]Jet Propulsion Laboratory, California Institute of Technology, Pasadena, California, USA.

0094-8276/11/2011GL048757

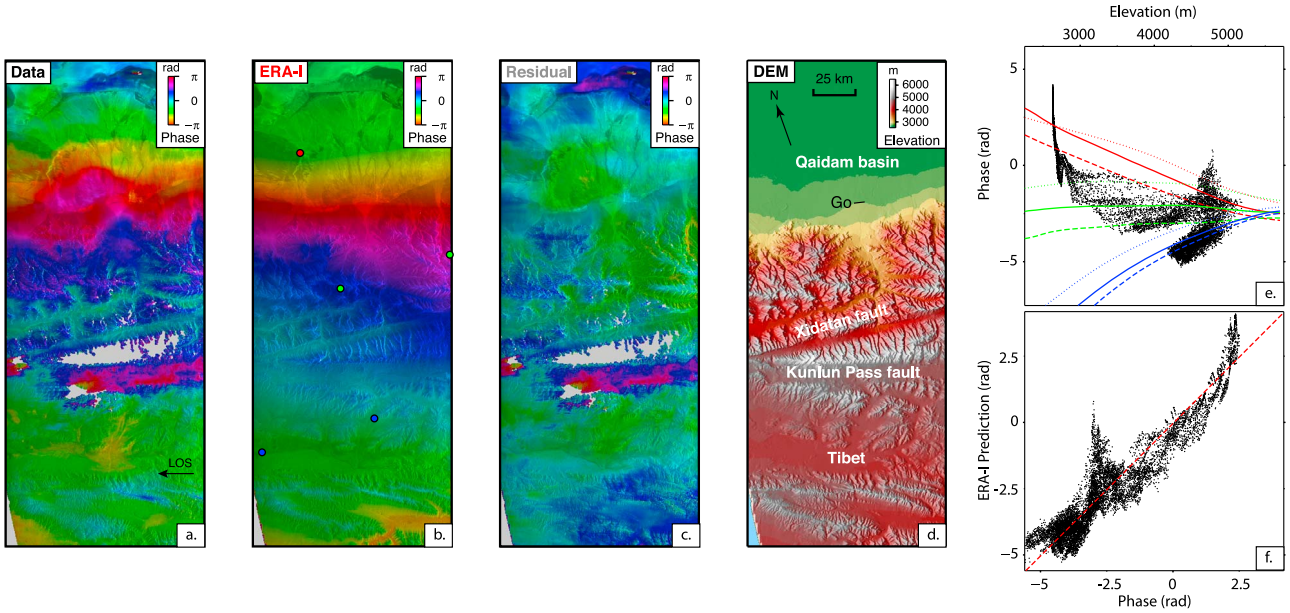

Figure 1. Example of interferogram and atmospheric correction across the Kunlun fault. (a) Flattened unwrapped interferogram from SAR acquisitions on 10-16-2006 and 11-20-2006, in radar geometry. (b) Corresponding stratified delay map predicted by ERA-I. Colored dots indicate ERA-I grid points location and correspond to colored delay functions in Figure 1e. (c) Residuals after correction of Figure 1a by Figure 1b. (d) SRTM Digital elevation model. Go: City of Golmud. (e) Black dots: pixel phase values as a function of elevation. Red, green, blue lines correspond to predicted delay functions of ERA-I grid points in red, green, blue on Figure 1b, located in the Qaidam basin (north, 2600 m to 2800 m), in the Kunlun range (center, 2800 m to 6000 m), on the Tibetan plateau (south, 4500 m to 5000 m), respectively. Continuous, dashed and dotted are for western, central and eastern point respectively. (f) Predicted delay values as a function of InSAR phase. Red dashed line indicates the unit correlation. Large deviations from the unit correlation correspond to the base of alluvial fans, likely affected by hydrologically-related effects. Correlation coefficient is 0.86.

maps from the ERA-I models outputs. We then validate our approach using ENVISAT C-band interferograms, highlighting the agreement between observed and modeled topography-dependent phase delays. We finally show that applying this method in areas of rough topography to remove the modeled atmospheric component of the phase from wrapped interferograms reduces the local phase variance and helps with unwrapping.

2. Atmospheric Phase Delay Modeling

[7] The LOS single path tropospheric delay $\delta L^s_{LOS}(z)$ at an elevation z is the integral of the air refractivity between the surface elevation z and an elevation of reference z_{ref} and is modeled as [*Berrada Baby et al.*, 1988]:

$$\delta L^s_{LOS}(z) = \frac{10^{-6}}{\cos(\theta)}\left\{\frac{k_1 R_d}{g_m}\left(P(z) - P(z_{ref})\right) + \int_z^{z_{ref}}\left(\left(k_2 - \frac{R_d}{R_v}k_1\right)\frac{e}{T} + k_3\frac{e}{T^2}\right)dz\right\}, \quad (1)$$

where θ is the local incidence angle, $R_d = 287.05$ J.kg^{-1}.K^{-1} and $R_v = 461.495$ J.kg^{-1}.K^{-1} are respectively the dry air and water vapor specific gas constants, g_m is a weighted average of the gravity acceleration between z and z_{ref}, P is the dry air partial pressure in Pa, e is the water vapor partial pressure in Pa, and T is the temperature in K. The constants are $k_1 = 0.776$ K.Pa^{-1}, $k_2 = 0.716$ K.Pa^{-1} and $k_3 = 3.75 \cdot 10^3$ K^2.Pa^{-1} [*Smith and Weintraub*, 1953]. z_{ref} is chosen as the height above which the delay is assumed to be nearly unchanged with time (typically 10000 m). The first term in equation (1) corresponds to the dry air component of the delay path, while the second term is related to air moisture.

[8] ERA-I is a global atmospheric model computed by the ECMWF based on a 4D-Var assimilation of global surface and satellite meteorological data [*Dee et al.*, 2011]. This re-analysis provides values of several meteorological parameters on a global ~75 km grid from 1989 to the present day, at 0 am, 6 am, 12 pm and 6 pm UT daily. The vertical stratification is described on 37 pressure levels, densely spaced at low elevation (interval of 25 hPa), with the highest level around 50 km (1 hPa). The pressure levels located under the local elevation of grid nodes are obtained by extrapolation.

[9] For each acquisition date, we select the ERA-I output that is the closest to the SAR acquisition time. We interpolate the temperature, water vapor and dry air partial pressure provided at each pressure level to predict the delay as a function of elevation $\delta L^s_{LOS}(z)$ on each ERA-I grid point in the vicinity of the radar scene. A bilinear interpolation in the horizontal dimensions and a spline interpolation along altitude is then applied to produce a map of the predicted delay. Total delay maps at epoch of acquisitions are then combined by pairs to produce differential delay maps corresponding to each interferogram. The use of the precise formulation of the single path LOS delay and of the profiles of temperature, water vapor and dry air partial pressure is of

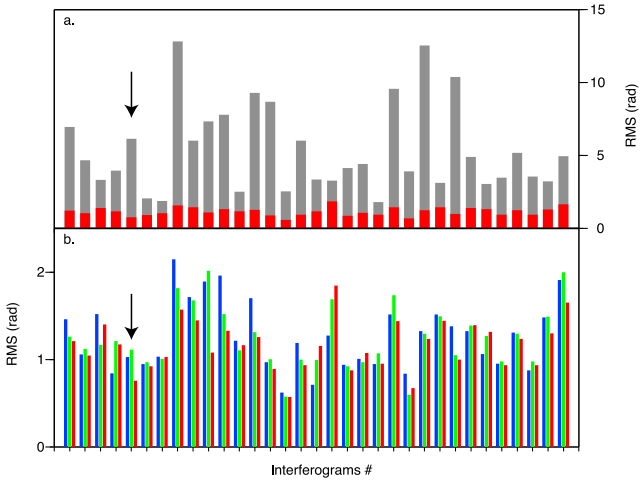

Figure 2. (a) RMS comparison of unwrapped interferograms corrected from the best fitting orbital plane (gray bars) and corrected from the full-grid ERA-I predicted atmospheric delay map (red bars). (b) RMS comparison of unwrapped interferograms corrected from empirical linear phase/elevation relationship (blue bars), corrected from atmospheric delay computed from one single ERA-I grid point (green bars) and corrected from the full-grid ERA-I predicted atmospheric delay map (red bars). The black arrow indicates interferogram shown on Figure 1.

importance to compute an accurate delay function, whereas surface measurements and approximate delay formulas prove to be insufficient [*Fournier et al.*, 2011].

3. Validation on Unwrapped Interferograms

[10] We validate our approach in the area of the left-lateral Kunlun fault, where no in-situ meteorological data is available. This fault separates the Qaidam basin to the north (~2500 m) from the Tibetan plateau to the south (~5000 m), following the eastern Kunlun range, whose highest peak reaches ~6000 m (Figure 1). Consequently, topography and interseismic deformation are correlated in this area and any empirical method based on phase/elevation relationship to describe the atmospheric phase delay would likely result in biased estimates of the fault slip rate.

[11] From 33 Envisat raw data on track 090 across the Kunlun fault, we generate, look 16 times, filter and unwrap 33 interferograms, using the NSBAS processing chain [*Doin et al.*, 2011] coupled with ROI_PAC [*Rosen et al.*, 2004]. As the Kunlun fault slip rate is about 1 cm/yr [*Wang et al.*, 2001; *Van Der Woerd et al.*, 2002], we only generate interferograms whose temporal baseline does not exceed 2 months (i.e., with negligible tectonic deformation signal). Modeled differential delay maps are subtracted from each interferogram. Orbital errors are then removed by adjusting a second-order polynomial surface to the residual.

[12] Figure 1 shows a comparison between unwrapped interferograms and modeled delay maps. The uncorrected, unwrapped interferogram, generated from two winter acquisitions reveals topography-related features. However, as shown on Figure 1e, the relationship between pixel phase and elevation is neither linear nor quadratic, suggesting a complex delay function. Nevertheless, a close examination of ERA-I predicted delay functions $\delta L^{s}_{LOS}(z)$ on the scene reveals that the pixel phase values agree with the predicted phase at the closest ERA-I grid point (Figure 1e). This indicates that most of this apparent complexity is due to a lateral variation of the delay/elevation relationship, that is correctly rendered by the ERA-I model. Figure 1f shows the good pixel-to-pixel correlation between observed and the 3D full-grid ERA-I modeled delay.

[13] After delay correction, the RMS noise in interferometric phase drops by 87% to a value of 0.75 rad. Strong, localized phase variations can be observed in the residual along the Kunlun Pass fault and in the Qaidam basin, to the north, and are likely due to hydrologically-related motion at the base of alluvial fans bounding the Kunlun range (Figure 1f). An additional example (Figure S1) and the comparison between observed and predicted local phase/elevation ratios (Figure S2) are presented in the auxiliary material.[1]

[14] The efficiency of the modeled delay corrections can be compared with two alternative methods: (1) data correction from the joint inversion of the linear phase/elevation ratio together with residual orbital errors [*Cavalié et al.*, 2008], (2) data correction from the delay function computed from a single ERA-I grid point chosen as the one corresponding to the lowest elevation within the scene and from residual orbital errors. Initial and residual RMS are shown on Figure 2. The mean RMS reduction is similar with the three methods, (1) 71% (1.26 rad), (2) 71% (1.24 rad) while the 3D full-grid ERA-I correction gives 73% (1.15 rad). 3D full-grid ERA-I corrections in areas with broad elevation ranges can therefore be systematically applied to remove trade-offs between APS and deformation.

4. Improving the Interferometric Phase Unwrapping

[15] Correcting InSAR data using independent meteorological constraints is also useful to curb the impact of phase ambiguities and improve the reliability of interferogram unwrapping in regions of rough topography. We now focus on a track spanning, from north to south, the southern margin of the Tibetan plateau (~5000 m elevation), the Himalayan range (with elevations greater than 6000 m), and the Indo-Gangetic basin (elevation ~0 m) (Figure 3). The Himalayan range is an active collision belt, characterized by low-angle thrusting of the Indian lithosphere under the Tibetan plateau. GPS and levelling studies reveal that present-day convergence rate accommodated across the Himalayan range reaches 20 mm/yr, resulting in a band of interseismic surface uplift oriented parallel to the range, with a maximum rate reaching about 7 mm/yr around the latitude of the High Range [*Bilham et al.*, 1997; *Bettinelli et al.*, 2006]. The vertical component of the interseismic strain field is consequently expected to be partly correlated with elevation, and may therefore be difficult to discriminate from stratified atmospheric effects.

[16] In addition to this issue, a significant pitfall faced by InSAR studies in the Himalayas is the low coherence on the slopes of the mountain range, due to geometric decorrelation. Furthermore, changes of the stratification of the troposphere between epochs of radar data acquisitions result in large fringe gradients in areas of steep topographic slopes

[1] Auxiliary materials are available in the HTML. doi:10.1029/2011GL048757.

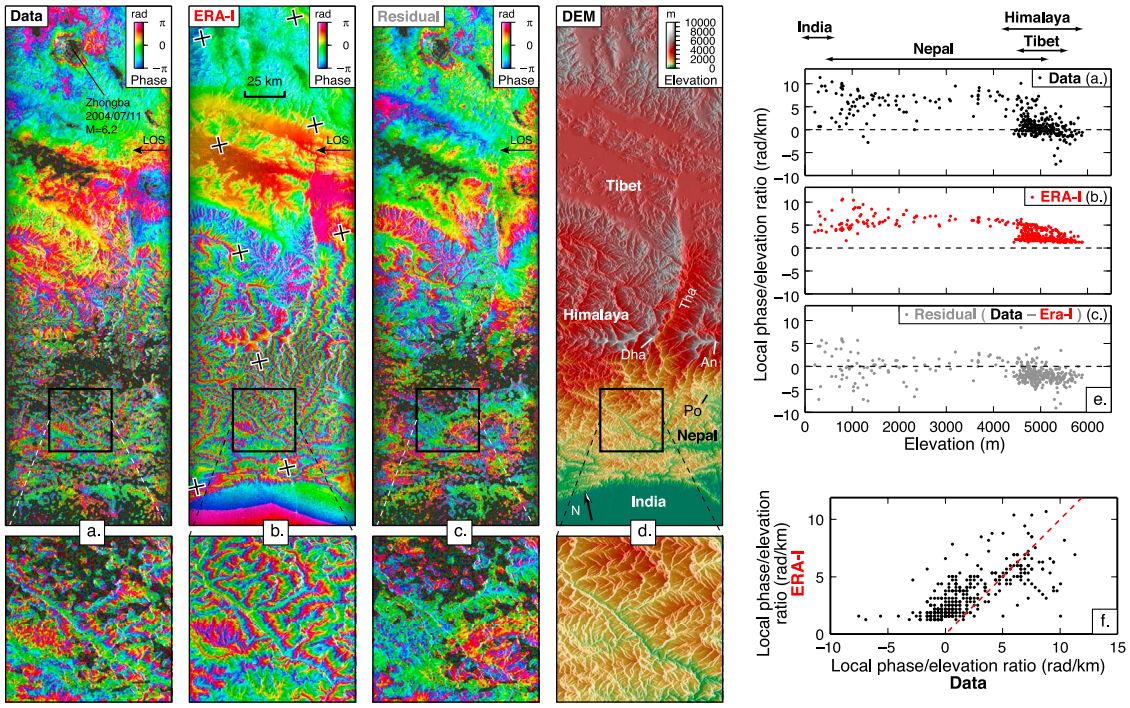

Figure 3. Example of interferogram and atmospheric correction across the Himalaya. (a) Wrapped interferogram from SAR acquisitions on 17-03-2004 and 08-09-2004, in radar geometry. (b) Corresponding stratified delay map predicted from ERA-I data. Dark crosses are ERA-I grid locations. (c) Residual after subtraction of Figure 3b from Figure 3a. (d) SRTM digital elevation model (DEM). Dha: Dhaulagiri (8167 m); An: Annapurna I (8091 m); Po: city of Pokhara; Tha: Thakkhola graben. Inset below each map shows a blowup of the region indicated by the black squares. (e) Observation (top, black), full-grid ERA-I prediction (middle, red) and residuals after ERA-I correction (bottom, grey) for local phase/elevation ratios computed in moving windows spanning the wrapped interferograms. Dashed line shows zero mean phase/elevation ratio. (f) Observed (x-axis) versus predicted (y-axis) phase/elevation ratios computed in each moving window in interferograms in Figures 3a and 3b, respectively. The red dashed line indicates the unit correlation. Correlation coefficient if 0.67.

(Figure 3a). This is particularly important at the southern side of the Himalaya where river incision produces rough relief (Figure 3d). Therefore, in such areas, downlooking the interferograms to improve the coherence generally leads to poor results, because of aliasing of these strong atmospheric gradients. As a consequence, correction of stratified tropospheric delay prior to interferogram downlooking and unwrapping is necessary in this particular setting.

[17] We combine 29 ENVISAT acquisitions between 2003 and 2010 into 35 interferograms with temporal baselines between 35 days and 3.5 years, and perpendicular baselines between 3 m and 389 m (an example is shown in Figure 3). Interferograms are downlooked by a factor 4 in range, and 20 in azimuth (Figure 3a). Wrapped interferograms are corrected from the stratified APS using the method presented in Section 2: we compute 3D full-grid ERA-I delay maps (Figure 3b), which are then wrapped and subtracted from the interferograms (Figure 3c). We estimate the local phase/elevation ratio in a series of 15 km-wide moving windows spanning the swath on both corrected and original interferogram to estimate the quality of that correction. Corrections derived from ERA-I lead, in most cases, to a significative decrease of the average phase gradient in the Himalaya, resulting in a spectacular reduction of the density of topography-related fringes, especially on the southern slopes of the range below the elevation of 4000 m (Figure 3e). Within our dataset, the absolute value of local phase/elevation ratios is decreased from 3.1 rad/km to 1.1 rad/km in average, which corresponds to a reduction from 2.5 to 0.8 of the total number of phase cycles across the 5000 m topographic step between Tibet and India (Figure S3).

[18] In the context of the Himalayan range, the reduction of the absolute value of phase/elevation ratios achieved by ERA-I has two advantages: (1) A decreased phase gradient prevents aliasing during downlooking, and therefore improves the coherence of downlooked interferograms. (2) The reduced phase ambiguity across prominent topographic features decreases the risk of errors during unwrapping (note the sharp improvement in fringe continuity in Figure 3c compared to Figure 3a).

5. Discussion

[19] Correcting atmospheric delays using ERA-I reanalysis data has two advantages in areas where deformation and topography are correlated and no additional meteorological constraint is available: (1) No empirical adjustment of the delay functions is needed, thus the results are unbiased with respect to other sources of errors (e.g., orbital errors, atmospheric turbulence, DEM errors, unmodeled deformation). The use of an "a priori" ERA-I correction should therefore contribute to a better orbital ramp assessment (Figure S4). (2) While reducing biases in strain rates estimation with time series analysis or stacks [*Doin et al.*,

2009], the method also helps the unwrapping process in areas where the topography-related fringe rate is high. This will be even more useful for X-band interferograms. Next-generation interferometric processing chains should include global atmospheric model outputs to perform routine corrections of stratified tropospheric delays. The low computational cost of the method should make its application particularly straightforward for the handling of the large amount of data expected to emanate from future SAR missions, such as ESA's SENTINEL-1.

[20] From the coarse spatial (~75 km) and temporal (4 times daily) sampling of the ERA-I model, one would expect that only broad features of the stratified troposphere are corrected. Nevertheless, stratified tropospheric delay is related to topography and therefore corrections of densely spaced fringe patterns are possible with an accurate DEM. However, correcting for the contribution of the turbulent troposphere would require a much denser spatial and temporal sampling of meteorological parameters. Until such improvements are achieved, one needs to assume atmospheric turbulence is random in space and time and mitigation of this effect requires the use of numerous acquisitions.

6. Conclusion

[21] In this study, we show the benefits of using global atmospheric model outputs to estimate first-order atmospheric phase delay and correct interferograms. Such corrections reduce biases in strain rates estimations and help the unwrapping process.

[22] The ability of atmospheric models to predict the atmospheric phase delay over continental areas has been demonstrated [*Elliott et al.*, 2008; *Doin et al.*, 2009; *Grandin*, 2009; *Pinel et al.*, 2011; this study]. However, predictions could be less accurate over coastal areas, where temporal fluctuations of the atmospheric delay and atmospheric turbulences are usually stronger [*Doin et al.*, 2009]. The ever-increasing quality and resolution of global atmospheric reanalysis and the expanding amount of SAR acquisitions planned by space agencies in the next decades are strong incentives to adopt such atmospheric corrections as a systematic step in the processing of radar interferometry data.

[23] **Acknowledgments.** The SAR data set was provided by the European Space Agency (ESA) in the framework of the Dragon program (projects ID 2509 and 5305). This program also partly supported R. Jolivet and R. Grandin's work, through the Young Scientist fellowship. Funding was provided by the French Agence Nationale pour la Recherche (EFIDIR, project ANR-07-MDCO-04) and Institut National des Sciences de l'Univers (Risk, PNTS). Postdoctoral fellowship for R. Grandin was provided by Centre National d'Études Spatiales. Part of G. Peltzer's contribution was done at the Jet Propulsion Laboratory, California Institute of Technology under contract with NASA. We thank two anonymous reviewers for their constructive comments.

[24] The Editor thanks Zhenhong Li and an anonymous reviewer for their assistance in evaluating this paper.

References

Beauducel, F., P. Briole, and J.-L. Froger (2000), Volcano-wide fringes in ERS synthetic aperture radar interferograms of Etna (1992–1998): Deformation or tropospheric effect?, *J. Geophys. Res.*, *105*, 16,391–16,402, doi:10.1029/2000JB900095.

Berrada Baby, H., P. Golé, and J. Lavergnat (1988), A model for the tropospheric excess path length of radio waves from surface meteorological measurements, *Radio Sci.*, *23*, 1023–1038.

Bettinelli, P., J.-P. Avouac, M. Flouzat, F. Jouanne, L. Bollinger, P. Willis, and G. R. Chitrakar (2006), Plate motion of India and interseismic strain in the Nepal Himalaya from GPS and DORIS measurements, *J. Geod.*, *80*, 567–589, doi:10.1007/s00190-006-0030-3.

Biggs, J., T. Wright, Z. Lu, and B. Parsons (2007), Multi-interferogram method for measuring interseismic deformation: Denali fault, Alaska, *Geophys. J. Int.*, *170*(3), 1165–1179, doi:10.1111/j.1365-246X.2007.03415.x.

Bilham, R., K. Larson, and J. Freymueller (1997), GPS measurements of present-day convergence across the Nepal Himalaya, *Nature*, *386*, 61–64, doi:10.1038/386061a0.

Cavalié, O., M.-P. Doin, C. Lasserre, and P. Briole (2007), Ground motion measurement in the Lake Mead area, Nevada, by differential synthetic aperture radar interferometry time series analysis: Probing the lithosphere rheological structure, *J. Geophys. Res.*, *112*, B03403, doi:10.1029/2006JB004344.

Cavalié, O., C. Lasserre, M. P. Doin, G. Peltzer, J. Sun, X. Xu, and Z. K. Shen (2008), Measurement of interseismic strain across the Haiyuan fault (Gansu, China), by InSAR, *Earth Planet. Sci. Lett.*, *275*(3–4), 246–257, doi:10.1016/j.epsl.2008.07.057.

Dee, D. P., et al. (2011), The ERA-Interim reanalysis: Configuration and performance of the data assimilation system, *Q. J. R. Meteorol. Soc.*, *137*(656), 553–597, doi:10.1002/qj.828.

Delacourt, C., P. Briole, and J. A. Achache (1998), Tropospheric corrections of SAR interferograms with strong topography: Application to Etna, *Geophys. Res. Lett.*, *25*, 2849–2852, doi:10.1029/98GL02112.

Doin, M. P., C. Lasserre, G. Peltzer, O. Cavalié, and C. Doubre (2009), Corrections of stratified tropospheric delays in SAR interferometry: Validation with global atmospheric models, *J. Appl. Geophys.*, *69*, 35–50, doi:10.1016/j.jappgeo.2009.03.010.

Doin, M. P., S. Guillaso, R. Jolivet, C. Lasserre, F. Lodge, G. Ducret, and R. Grandin (2011), Presentation of the small baseline NSBAS processing chain on a case example: The Etna deformation monitoring from 2003 to 2010 using Envisat data, paper presented at Fringe 2011 Workshop, Eur. Space Agency, Frascati, Italy, 19–23 Sept.

Elliott, J. R., J. Biggs, B. Parsons, and T. J. Wright (2008), InSAR slip rate determination on the Altyn Tagh Fault, northern Tibet, in the presence of topographically correlated atmospheric delays, *Geophys. Res. Lett.*, *35*, L12309, doi:10.1029/2008GL033659.

Fournier, T., M. E. Pritchard, and N. Finnegan (2011), Accounting for atmospheric delays in InSAR data in a search for long-wavelength deformation in South America, *IEEE Trans. Geosci. Remote Sens.*, *99*, 1–12, doi:10.1109/TGRS.2011.2139217.

Grandin, R. (2009), L'apport de la géodésie spatiale dans la compréhension du processus de rifting magmatique: L'exemple de l'épisode en cours en Afar Éthiopien, Ph.D. thesis, Inst. de Phys. du Globe de Paris, Paris.

Hanssen, R. F. (2001), *Radar Interferometry, Data Interpretation and Error Analysis*, *Remote Sens. Digital Image Process.*, vol. 2, Kluwer Acad., Dordrecht, Netherlands.

Li, Z., E. J. Fielding, P. Cross, and J.-P. Muller (2006a), Interferometric synthetic aperture radar atmospheric correction: GPS topography-dependent turbulence model, *J. Geophys. Res.*, *111*, B02404, doi:10.1029/2005JB003711.

Li, Z., E. J. Fielding, P. Cross, and J.-P. Muller (2006b), Interferometric synthetic aperture radar atmospheric correction: Medium Resolution Imaging Spectrometer and Advanced Synthetic Aperture Radar integration, *Geophys. Res. Lett.*, *33*, L06816, doi:10.1029/2005GL025299.

Lin, Y. N., M. Simons, E. A. Hetland, P. Muse, and C. DiCaprio (2010), A multiscale approach to estimating topographically correlated propagation delays in radar interferograms, *Geochem. Geophys. Geosyst.*, *11*, Q09002, doi:10.1029/2010GC003228.

Onn, F., and H. A. Zebker (2006), Correction for interferometric synthetic aperture radar atmospheric phase artifacts using time series of zenith wet delay observations from a GPS network, *J. Geophys. Res.*, *111*, B09102, doi:10.1029/2005JB004012.

Pinel, V., A. Hooper, S. De la Cruz-Reyna, G. Reyes-Davila, M.-P. Doin, and P. Bascou (2011), The challenging retrieval of the displacement field from InSAR data for andesitic stratovolcanoes: Case study of Popocatepetl and Colima volcano, Mexico, *J. Volcanol. Geotherm. Res.*, *200*, 49–61, doi:10.1016/j.jvolgeores.2010.12.002.

Puysségur, B., R. Michel, and J.-P. Avouac (2007), Tropospheric phase delay in interferometric synthetic aperture radar estimated from meteorological model and multispectral imagery, *J. Geophys. Res.*, *112*, B05419, doi:10.1029/2006JB004352.

Remy, D., S. Bonvalot, P. Briole, and M. Murakami (2003), Accurate measurements of tropospheric effects in volcanic areas from SAR interferometry data: Application to Sakurajima volcano (Japan), *Earth Planet. Sci. Lett.*, *213*, 299–310, doi:10.1016/S0012-821X(03)00331-5.

Rosen, P. A., S. Henley, G. Peltzer, and M. Simons (2004), Updated repeat orbit interferometry package released, *Eos Trans. AGU*, *85*(5), doi:10.1029/2004EO050004.

Schmidt, D. A., and R. Bürgmann (2003), Time-dependent land uplift and subsidence in the Santa Clara valley, California, from a large interferometric synthetic aperture radar data set, *J. Geophys. Res.*, *108*(B9), 2416, doi:10.1029/2002JB002267.

Smith, E. K., and S. Weintraub (1953), The constants in the equation for atmospheric refractive index at radio frequencies, *Proc. IRE*, *43*, 1035–1037.

Van Der Woerd, J., et al. (2002), Uniform postglacial slip-rate along the central 600 km of the Kunlun Fault (Tibet), from ^{26}Al, ^{10}Be, and ^{14}C dating of riser offsets, and climatic origin of the regional morphology, *Geophys. J. Int.*, *148*(3), 356–388, doi:10.1046/j.1365-246x.2002.01556.x.

Wadge, G., et al. (2002), Atmospheric models, GPS and InSAR measurements of the tropospheric water vapour field over Mount Etna, *Geophys. Res. Lett.*, *29*(19), 1905, doi:10.1029/2002GL015159.

Wang, Q., et al. (2001), Present-day crustal deformation in China constrained by global positioning system measurements, *Science*, *294*(5542), 574–577, doi:10.1126/science.1063647.

Webley, P. W., R. M. Bingley, A. H. Dodson, G. Wadge, S. J. Waugh, and I. N. James (2002), Atmospheric water vapour correction to InSAR surface motion measurements on mountains: Results from a dense GPS network on Mount Etna, *Phys. Chem. Earth*, *27*, 363–370, doi:10.1016/S1474-7065(02)00013-X.

Williams, S., Y. Bock, and P. Fang (1998), Integrated satellite interferometry: Tropospheric noise, GPS estimates and implications for interferometric synthetic aperture radar products, *J. Geophys. Res.*, *103*, 27,051–27,067, doi:10.1029/98JB02794.

Zebker, H. A., P. A. Rosen, and S. Hensley (1997), Atmospheric effects in interferometric synthetic aperture radar surface deformation and topographic maps, *J. Geophys. Res.*, *102*, 7547–7563, doi:10.1029/96JB03804.

M.-P. Doin and R. Grandin, Laboratoire de Géologie, Ecole Normale Supérieure, 45 rue Lhomond, F-75005 Paris CEDEX, France.

R. Jolivet and C. Lasserre, Institut des Sciences de la Terre, Université Joseph Fourier, BP 53, F-38041 Grenoble CEDEX, France.

G. Peltzer, Department of Earth and Space Sciences, University of California, Los Angeles, CA 90095, USA.